ELSEVIER

Turbulent characteristics of the flow in an axially rotating pipe

Shigeki Imao and Motoyuki Itoh
Department of Mechanical Engineering, Nagoya Institute of Technology, Gokiso-cho, Showa-ku, Nagoya, Japan

Takeyoshi Harada
Mitsubishi Heavy Industries Co. Ltd., Nagoya, Japan

This study examines the effects of the swirl driven by a rotating pipe wall on turbulent flow characteristics. Velocity measurements were performed at Reynolds number Re=20000 using a single-component laser-Doppler velocimetry (LDV) operated in forward scatter. The test apparatus was refractive index matched, allowing measurement of the turbulent fluctuation velocities and Reynolds shear stresses of the flow in an axially rotating pipe. The results indicate that the intensity of turbulence in the rotating pipe decreases gradually with an increase in pipe rotation due to the stabilizing effect of the centrifugal force. The Reynolds shear stresses decrease markedly as compared with turbulence intensity, and momentum transfer by turbulence is suppressed strongly in the rotating pipe. Based on the experimental results, the relationship between the reduced mixing length and Richardson number is verified for the turbulent flow in the rotating pipe. Data on skewness and flatness factors, time records of velocity fluctuation, and their power spectra are also presented and show the change in turbulence structures.

Keywords: turbulence; pipe flow; swirling flow; Reynolds stress; laser-Doppler velocimetry; rotating pipe

Introduction

When a pipe flow is subjected to axial rotation, a tangential velocity component is given to the flow by the moving wall, and the velocity distribution and turbulent characteristics of the flow differ from those observed in a stationary pipe. Experimental data about these swirling flows are important for code validation and of value as references for the inlet flow of fluid machines.

Hydraulic losses and mean velocity profiles of the flow in an axially rotating pipe have been studied by several investigators, including the present authors. Experimental results showed that pipe rotation had two countereffects on the flow, stabilizing or destabilizing. When the Reynolds number is small and the flow is laminar, pipe rotation destabilizes the flow, and the spiral waves appear (Imao et al. 1989, 1992). On the other hand, pipe rotation has stabilizing effects in the turbulent region, in which the reduction in the hydraulic loss and the deformation of the axial velocity profile into a shape similar to the laminar one were obtained by White (1964), Murakami and Kikuyama (1980), and Imao (1981). The present study is concerned with the latter effect in the turbulent region.

For turbulent boundary layers developed in an axially rotating pipe, Kikuyama et al. (1983a) measured the time-mean velocities and Reynolds stress components by the use of hot wire probes and showed that the intensity of turbulence in the rotating pipe decreased ultimately below that in a stationary pipe. Kikuyama et al. (1983b) applied the mixing length model modified by the Richardson number to predict the laminarization phenomena of swirling flow in the rotating pipe. Numerical computations were made by Hirai et al. (1988) applying three kinds of turbulence models, and the computations were compared with the experiments in terms of mean velocity profiles. To help explain the behaviour of the stabilizing process due to the swirl, and to examine the applicability of the turbulence models to the swirling flow, it is desirable to obtain systematic data including velocity distributions and stress components of the fully developed flow in an axially rotating pipe. However, turbulent characteristics of this flow have never been measured and are, therefore, unknown. The present authors measured mean velocity profiles, distributions of five components of the Reynolds stress, and velocity fluctuations and their power spectra of the flow in an axially rotating pipe by the use of a laser-Doppler velocimeter (LDV). In the present study, the refractive index of the working fluid was matched with that of the acyclic rotating pipe, which enabled us to measure velocity and stress components accurately. Using the experimental results, the relationship between the mixing length and Richardson number proposed by Bradshaw (1969) was examined. The results obtained here give useful data for investigators

Address reprint requests to S. Imao, Department of Mechanical Engineering, Nagoya Institute of Technology, Gokiso-cho, Showa-ku, Nagoya 466, Japan.

Received 18 January 1995; accepted 16 April 1996

Int. J. Heat and Fluid Flow 17: 444–451, 1996

655 Avenue of the Americas, New York, NY 10010

0142-727X/96/$15.00
PII S0142-727X(96)00057-0

studying the swirling flow. Some of them also have ramifications for the general problem of transition and turbulent structure.

Experimental apparatus and procedure

Figure 1 shows the experimental apparatus. A circulation system was employed, and a honed stainless pipe of 30.0-mm inside diameter was used for the rotating pipe. The fluid discharged from a centrifugal pump was introduced into the rectifying section through a 180° bend. After the tangential velocity component was eliminated, and the flow was made homogeneous over the inlet section of the rotating pipe by screens, the flow was throttled by the nozzle in a ratio of 11:1, which made the velocity profile at the inlet section of the rotating pipe almost uniform. The distance from the pipe inlet to the measuring section could be changed by moving the rectifying section. Figures 2(a) and (b) show the LDV system and the measuring section. The measuring section was composed of an acrylic pipe with the same inside diameter as the stainless pipe, and it was enclosed in an outer, square-sided containment vessel. The volume between the measuring section and the outer containment was filled with a working fluid, which was selected to have a refractive index equal to that of the acrylic pipe. The match of refractive indices was achieved by controlling the concentration of sodium iodide (NaI) water solution. If the refractive index of the working fluid differs from that of the pipe, it is impossible to measure turbulent shear stresses and a radial velocity component near the wall by a one-component LDV. Figure 2(c) shows how to measure tangential and radial velocity components. A microcomputer and pulse motors were used to move the optical system horizontally and vertically in the cross section. The LDV used here was a one-component, forward scatter system, operating with a He–Ne laser. The focal length is 120 mm, and the dimensions of the measuring volume, which is ellipsoid, are 0.5 mm in the laser light axis direction and 0.1 mm in the normal direction. Concerning the spatial resolutions, it differs a little by the orientation of the measuring volume of the LDV. However,

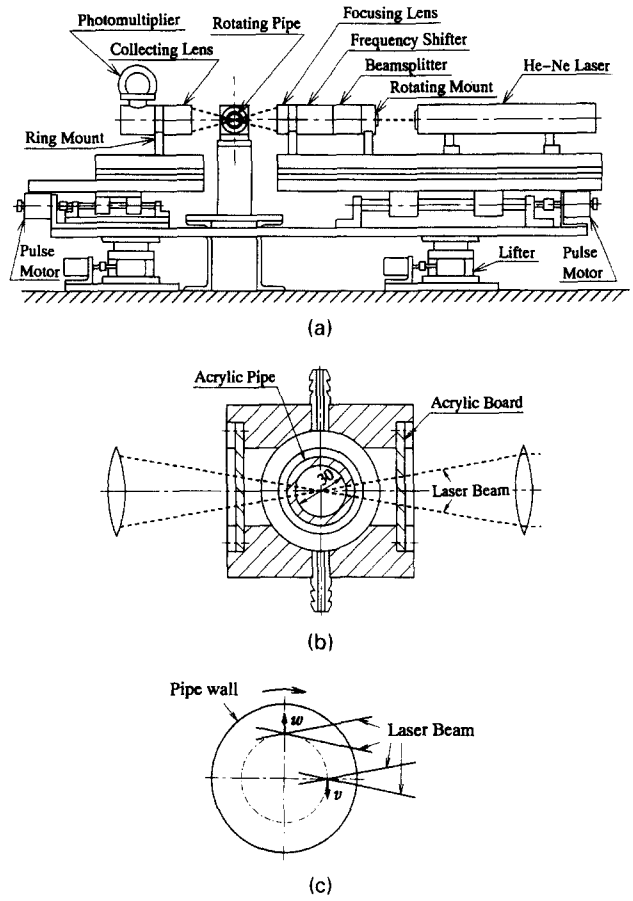

Figure 2 (a) LDV system. (b) Details of measuring section. (c) Measurement of tangential and radial velocity components

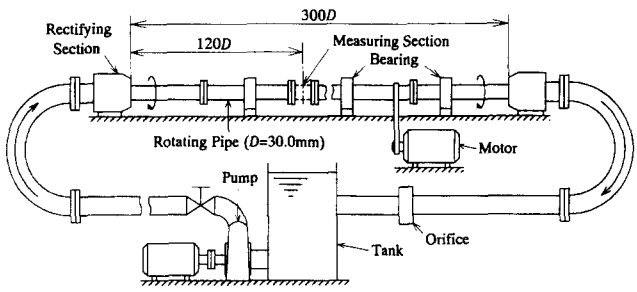

Figure 1 Schematic outline of experimental apparatus

when the axial velocity components were measured in the horizontal plane and in the vertical plane, respectively, and were compared, there was little difference between them. Moreover, in this study there did not exist a steep velocity gradient so that the velocity component changed considerably in the measuring volume. Therefore, the difference in the spatial resolution is regarded as negligible. A single Brag cell was used to provide a net frequency shift. To measure velocity components by a one-component LDV, a laser beam plane (i.e., measuring plane) was rotated at 0°, ±45°, 90° orientations about the optical axis. Thus, Reynolds stress components $\overline{u^2}$, $\overline{v^2}$, $\overline{w^2}$, $\overline{uw}$, and $\overline{uv}$ could be obtained in addition to axial, tangential, and radial components

Notation

D	pipe diameter, 30.0 mm
k	wave number
l	mixing length
N	rotation rate, V_w/U_m
$q^2/2$	kinetic energy of turbulence, $(\overline{u^2}+\overline{v^2}+\overline{w^2})/2$
r	radial distance
R	pipe radius, $D/2$
Re	axial Reynolds number, DU_m/ν
Ri	Richardson number defined by Equation 3
U,V	time-mean velocity components in the z and θ directions, respectively
u,v,w	fluctuating velocity components in the z, θ, and r directions, respectively
U_m	mean axial velocity
V_w	tangential speed of the rotating pipe
z	axial distance from the inlet section of the rotating pipe

Greek

β	parameter in Equation 2
λ	friction factor
ν	kinematic viscosity of fluid

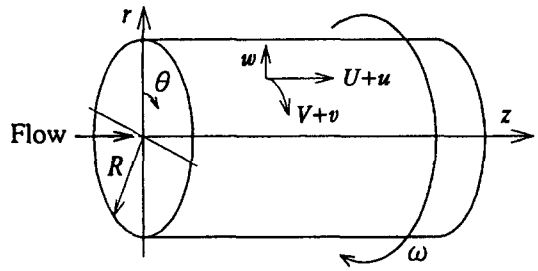

Figure 3 Coordinate system and velocities

of velocity. The LDV signals were processed using a counter-type processor. In general, signals obtained by LDV cannot be regarded as continuous data. In this study, however, the particle arrival rate was sufficiently high (always larger than 1000 1/s) for the signals to be regarded as continuous. Therefore, the digital output of the counter-type processor was once D/A converted, and then the analog data were sampled with sampling frequency 1 kHz by A/D converter, and data output was transferred to the memory of a microcomputer for analysis. Measurements were made for the axial Reynolds number Re = 20,000 and for the range of rotation rate $0 \leqq N \leqq 1$ at $z/D = 120$. The coordinate system is shown in Figure 3. The method's of Kline and McClintock (1953) was used to estimate the uncertainty for the measurements, and are given in the captions at the 95% confidence level.

Experimental results and discussion

Mean velocity profiles and friction factor

We measured mean velocity profiles at six cross sections; i.e., $z/D = 30$, 60, 90, 120, 160, 180, before this study. The results showed that the profiles remained unchanged downstream of $z/D = 120$, so we confirmed that the flow had been fully developed at $z/D = 120$ under the conditions examined here. Figure 4 shows velocity profiles at Re = 20000, $z/D = 120$. In this figure, axial and tangential velocity components and radial positions are made nondimensional by mean axial velocity, tangential speed of the rotating pipe, and pipe radius, respectively. When the pipe is rotated, axial velocity increases near the center and decreases near the wall, and the axial velocity profile gradually approaches a laminar shape with an increase in rotation rate, due to a stabilizing effect. The tangential velocity profile is not a forced-vortex type, but a concave one close to a parabolic curve $V/V_w = (r/R)^2$, even when the flow is fully developed. Similar results obtained by Imao (1981), Kikuyama et al. (1983b), Hirai et al. (1988), and Prandtl (1930) have suggested that a parabolic tangential velocity profile is a stable one from the viewpoint of the kinetic energy balance in the swirling flow. The fact that such a concave profile exists means that the tangential shearing stress is acting on the pipe wall even when the flow is developed.

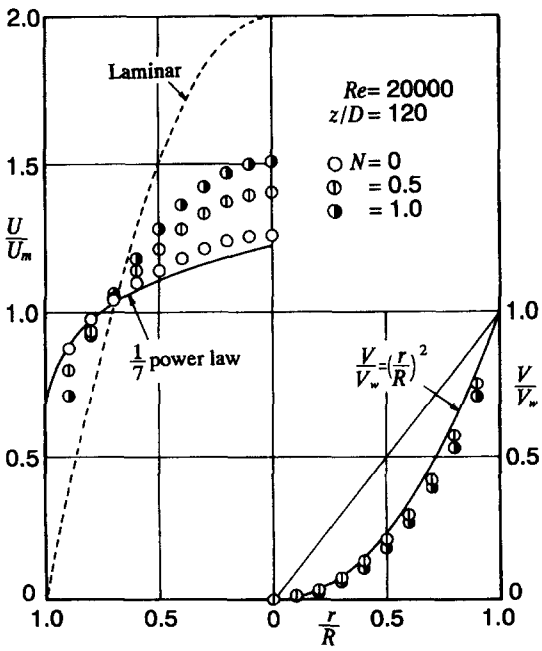

Figure 4 Time-mean velocity profiles (uncertainties in r/R are ±1%, and in U/U_m and V/V_w are ±2%)

Friction factors at Re = 20000 are shown in Figure 5. The friction factor λ is defined as

$$\lambda = \Delta p \Big/ \left(\frac{L}{D} \frac{\rho U_m^2}{2} \right),$$

where Δp is the pressure drop between the two pressure tappings situated at $z/D = 120$ and 180. Pressure tappings were provided in a narrow stationary ring 5-mm in length between two rotating sections (Imao et al. 1992). When the pipe is rotated, the λ values are smaller than those for stationary pipe, and they become smaller with an increase of N. The reduction in λ is 20% at $N = 0.5$, and 40% at $N = 1$, respectively, compared with the nonrotating state.

Reynolds stresses

Before the measurement of stress components in the rotating pipe, we performed a preliminary measurement of Reynolds stress of turbulent flow in a stationary pipe to check the measurement accuracy. The measured stress components were compared with the data obtained by Laufer (1954) and Lawn (1971) in Figure 6. In this figure, U_τ is the friction velocity calculated from the measured value of pressure drop. The agreement between the stress components measured in this study and those obtained by Laufer or Lawn was satisfactory, which demonstrates the accuracy and reliability of the present measurement. Figure 7 shows the distributions of turbulence intensity. It may be seen that every component of turbulent intensity decreases with an increase in rotation rate, although the rate of reduction is not so

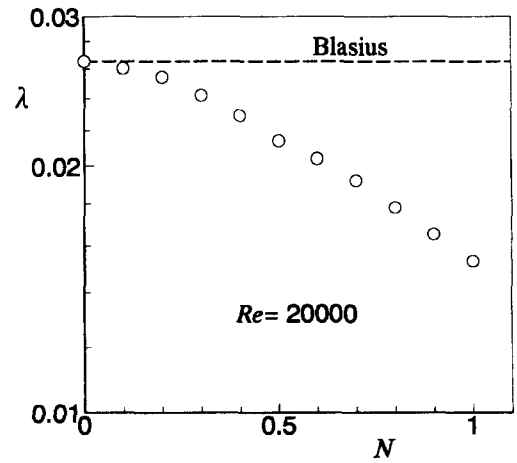

Figure 5 Friction factor (uncertainties in N and λ are ±0.5% and ±3%, respectively)

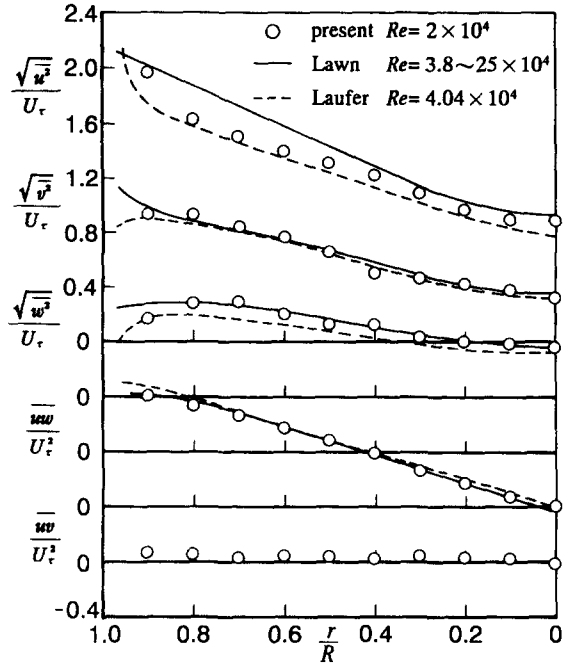

Figure 6 Reynolds stress profile in a stationary pipe (uncertainties in $\sqrt{\overline{u^2}}/U_\tau$, $\sqrt{\overline{v^2}}/U_\tau$ and $\sqrt{\overline{w^2}}/U_\tau$ are ±3%, and in $\overline{uw}/U_\tau^2$ and $\overline{uv}/U_\tau^2$ are ±5%)

remarkable. Among the three components $\sqrt{\overline{u^2}}$, $\sqrt{\overline{v^2}}$, and $\sqrt{\overline{w^2}}$, the rate of reduction in the radial component is the largest, which means that the pipe rotation most markedly suppresses the radial component of turbulent fluctuation. In this paper, U_m is used instead of U_τ as the parameter for normalization. The reason for it is as follows. When the pipe is rotated, the flow is stabilized, and the friction loss is not as great with rotation as it is without rotation, which corresponds to the decrease in the value of U_τ. If U_τ is used for normalization, the normalized

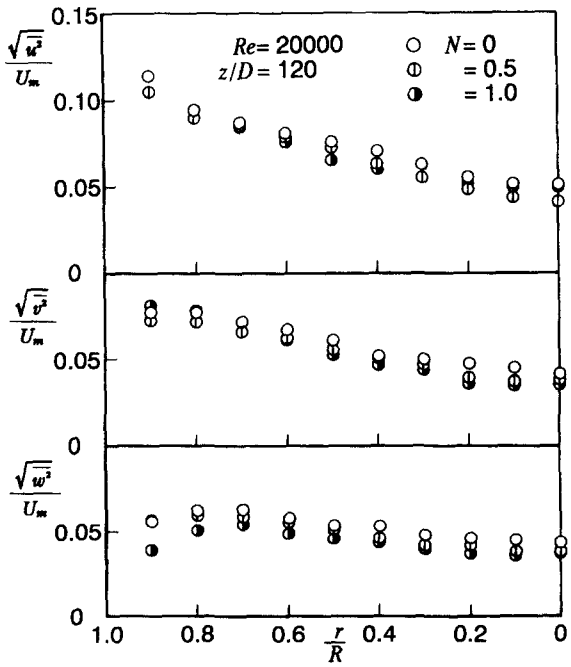

Figure 7 Distributions of turbulence intensity (uncertainties in $\sqrt{\overline{u^2}}/U_m$, $\sqrt{\overline{v^2}}/U_m$ and $\sqrt{\overline{w^2}}/U_m$ are ±3%)

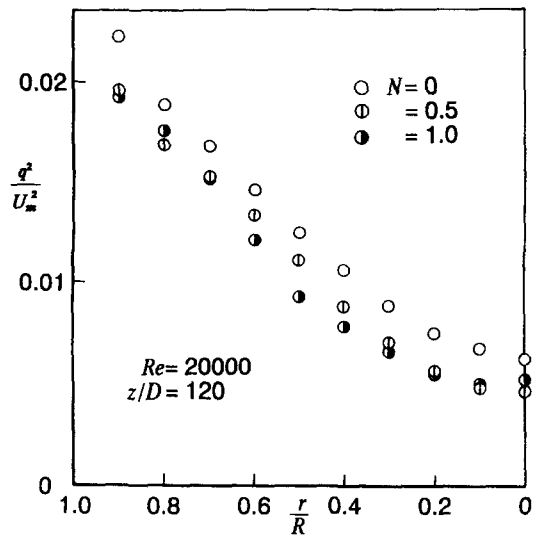

Figure 8 Distributions of turbulent energy (uncertainties in q^2/U_m^2 are ±3%)

Reynolds stress components in the rotating pipe become large, and it is impossible to look into the effect of pipe rotation directly. In addition, there exists tangential shearing stress in the rotating pipe, as mentioned earlier. Under these circumstances, it is not clear whether U_τ should be used for the velocity scale as the case in stationary pipe. Therefore, U_m is used instead of U_τ. Figure 8 shows the distributions of (twice) the kinetic energy of turbulent fluctuation $q^2 = \overline{u^2} + \overline{v^2} + \overline{w^2}$. Turbulent kinetic energy in the rotating pipe falls below that in the stationary pipe in every radial position. Here, we introduce total turbulent energy flux defined by Equation 1 to investigate the rate of reduction in turbulent kinetic energy over the cross section.

$$T_{\text{tef}} = \int_0^R \frac{1}{2}\rho q^2 \cdot U \cdot 2\pi \, \text{rdr} \tag{1}$$

Figure 9 shows the nondimensional total turbulent energy flux divided by $\rho U_m^3 \pi R^2$. With an increase in rotation rate, this quantity decreases gradually, and the rate of turbulent energy transport in the axial direction is reduced 18% at $N = 1$. From the measurement of the pressure drop in the rotating pipe, one

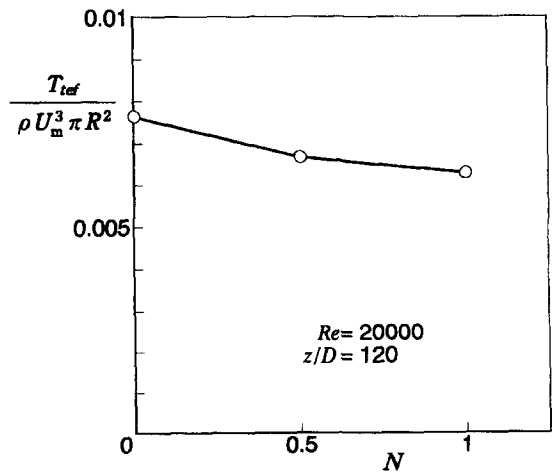

Figure 9 Total turbulent energy flux (uncertainties in $T_{\text{tef}}/\rho U_m^3 \pi R^2$ are ±5%)

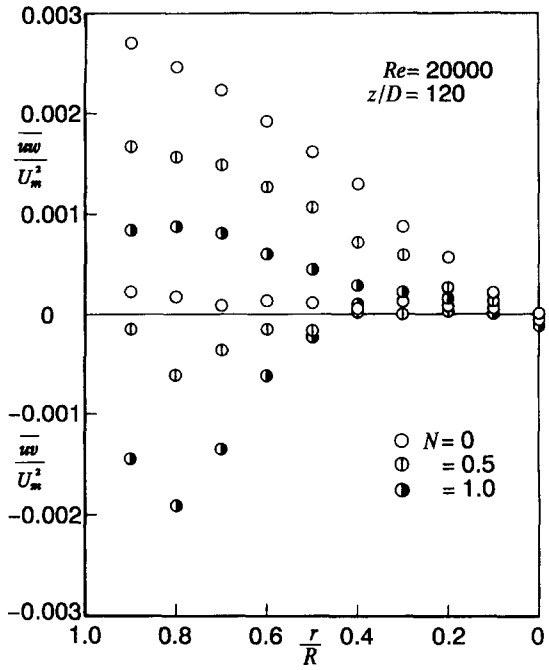

Figure 10 Distributions of turbulent shear stress (uncertainties in $\overline{uw}/U_m^2$ and $\overline{uv}/U_m^2$ are ±5%)

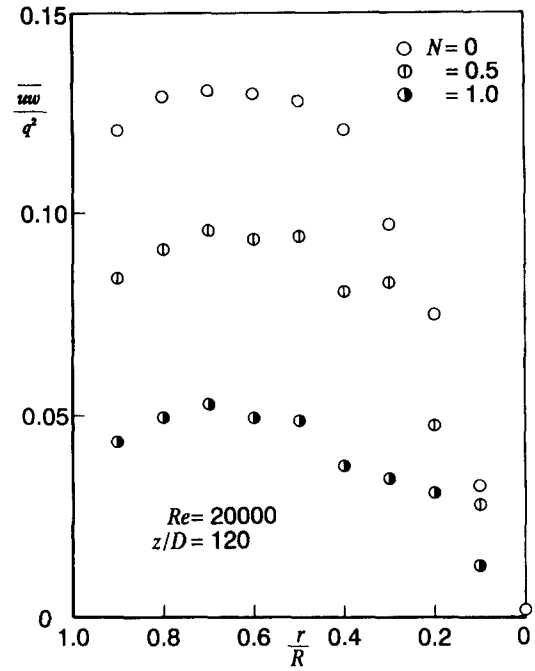

Figure 11 Structure parameter (uncertainties in $\overline{uw}/q^2$ are ±5%)

of the authors (Imao 1981) deduced that at this Reynolds number, a laminarization or retransition phenomenon could be seen clearly when the rotation rate was greater than three. Therefore, a drastic change in turbulence intensity is expected to occur when the rotation rate exceeds three.

In contrast to turbulence intensity, turbulent shear stresses change considerably when the pipe is rotated. Figure 10 shows turbulent shear stresses $\overline{uw}$ and $\overline{uv}$. With an increase in rotation rate, the $\overline{uw}$ component, which acts on the plane parallel to the pipe wall, decreases in every radial position, and at $N = 1$, its value becomes only about one-third of that without rotation. More detailed measurements showed that the reduction in the $\overline{uw}$ component was almost linear with an increase in N, as was the case in the pressure drop. As for the stress component $\overline{uv}$, which acts on the plane perpendicular to the pipe axis, it becomes negative at the large radial position, its absolute value increasing with an increase in N. A qualitative explanation for why the $\overline{uv}$ component becomes negative is as follows. In the rotating pipe, the axial velocity U decreases and the tangential velocity V increases, both monotonically, from the pipe center toward the pipe wall, as shown in Figure 4. Therefore, the signs of the velocity gradients dU/dr and dV/dr are opposite. If the fluctuation in a radial direction is considered, one component of the fluctuating velocity (u or v) is positive and another (v or u) negative. Consequently, the $\overline{uv}$ component, which is the cross-correlation of axial and tangential velocity fluctuations, is likely to be negative. In view of the transport equation of $\overline{uw}$, the production terms of the shearing stress $\overline{uw}$ can be written

$$-\overline{w^2}\frac{\partial U}{\partial r} + \overline{uv}\frac{V}{r}$$

(Hirai et al. 1988; Kitoh 1991). The results can be interpreted to mean that the reduction of the turbulent momentum flux $\rho\overline{uw}$ is caused by the negative production term $\overline{uv}V/r$ when the pipe is rotated.

Figure 11 shows the ratio of shear stress magnitude (in the plane parallel to the wall) to twice the turbulent kinetic energy, which is commonly called the structure parameter. Here the $\overline{vw}$ component is assumed to be zero, because the flow has been fully developed. In comparing the nearly constant value of $\overline{uw}/q^2$ in the region $0.5 \leqq r/R \leqq 0.8$ obtained here for $N = 0$ with those obtained by Laufer (1954), they were found to be 8% lower. Although the cause of this discrepancy is not clear, it may be due to a difference in the Reynolds number. With an increase in rotation rate, the ratio $\overline{uw}/q^2$ drops remarkably, so that turbulence structure in the rotating pipe becomes the one where momentum transfer by turbulence is suppressed. While this study is limited in the rotation rate not exceeding one, in the previous study (Imao 1981) a remarkable reduction in the normal stresses was found to occur when the rotation rate was greater than three. Therefore, it is deduced that the pipe rotation reduces the shearing stress mainly when the rotation rate is small and reduces the normal stresses when the rotation rate is large.

Mixing length

Figure 12 shows the mixing length obtained from the measured Reynolds stress $\overline{uw}$ and the axial velocity gradient dU/dr. It is seen that the reduction in the mixing length is quite remarkable, even when the rotation rate is 0.5, and the mixing length decreases still more with an increase in rotation rate. This fact once more shows that the momentum transfer by turbulent motion is suppressed due to the stabilizing effect of the centrifugal force. By analogy with the effects of buoyancy and centrifugal force, Bradshaw (1969) has proposed that the mixing length l in swirling flows could be expressed as

$$l = l_0(1 - \beta\,\mathrm{Ri}) \tag{2}$$

where β is a constant, l_0 is the mixing length in a flow with no rotation effect, and Ri is the Richardson number defined by

$$\mathrm{Ri} = \frac{\dfrac{2V}{r^2}\dfrac{\partial(rV)}{\partial r}}{\left(\dfrac{\partial U}{\partial r}\right)^2 + \left(\dfrac{r\partial(V/r)}{\partial r}\right)^2} \tag{3}$$

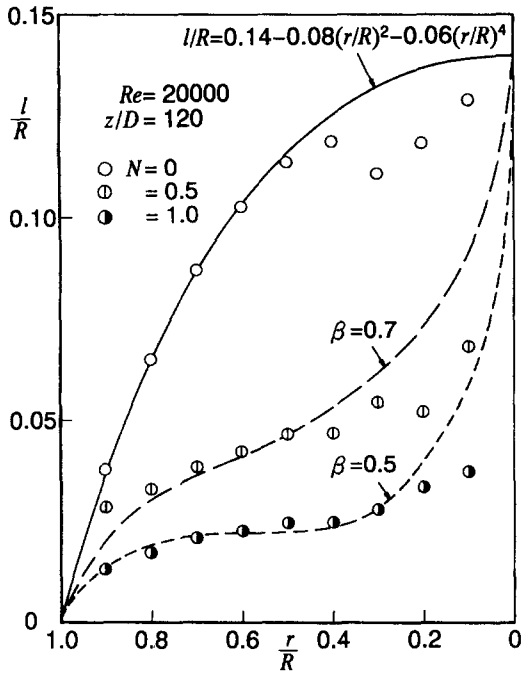

Figure 12 Mixing length (uncertainties in l/R are ±10%)

In the rotating pipe, the value of the angular momentum rV increases with the radial distance r, and hence Ri becomes positive. The positive value of Ri means that the flow is stabilized. Using the value of Ri calculated by Equation 3, the values of the mixing length at $N = 0.5$ and 1.0 can be evaluated, and the results are compared with the experiments in Figure 12. Here the constant β in the Monin–Oboukhov relation 2 is taken as 0.7 and 0.5 for two rotations rates, respectively, which are less than the value reported by many workers for a flow through a curved or rotating channel ($\beta = 2 \sim 7$). It is seen that the calculated values agree with the experiments.

Turbulent fluctuations

Here, velocity fluctuations in each direction are studied in detail. Figure 13 shows the time records of the radial velocity fluctuation and its probability density function at $r/R = 0.9$. As mentioned earlier, the fluctuating velocity component in the radial direction is mot suppressed by the pipe rotation among three components, and it can readily be seen from this figure that the amplitude of the fluctuation is noticeably decreased at $N = 1$ and that the fluctuation becomes intermittent. The probability density function also shows a change. The skewness factor S and the flatness factor F of the radial velocity fluctuation are shown in Figures 14 and 15, respectively. The values of S, which is negative in the stationary pipe, approach zero with an increase in rotation rate in every radial position, so that fluctuations with large negative value in the radial direction, such as ejection from near the wall, are depressed in the rotating pipe. The values of F increase with an increase in rotation rate. It is particularly remarkable at the large radial position. Therefore, the fluctua-

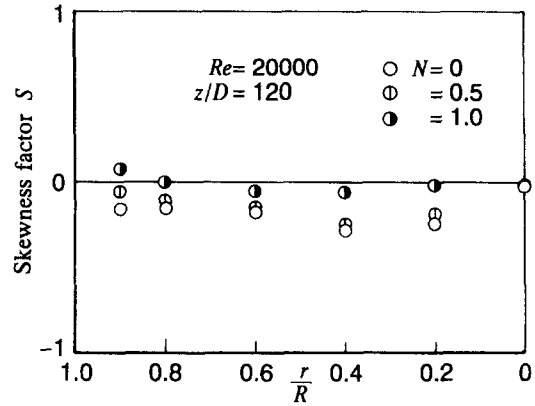

Figure 14 Skewness factor of radial velocity fluctuation $S = \overline{w^3}/(\overline{w^2})^{3/2}$ (uncertainties in S are ±3%)

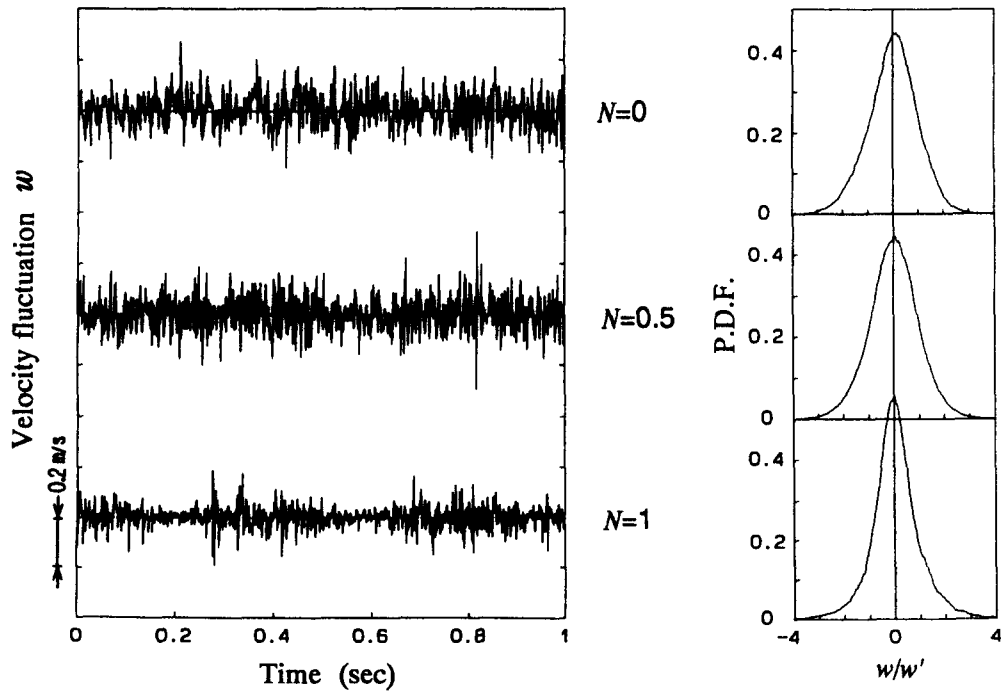

Figure 13 Time records of radial velocity fluctuation and their probability density function (Re=20000, z/D=120, r/R=0.9)

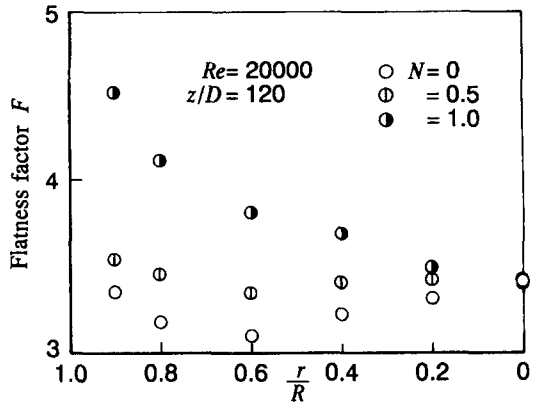

Figure 15 Flatness factor of radial velocity fluctuation $F = \overline{w^4}/(\overline{w^2})^2$ (uncertainties in F are ±3%)

tion in the radial direction is growing intermittent due to the stabilizing effect of pipe rotation in the outer region of the pipe.

Figures 16(a) and (b) show time records of the axial and the tangential velocity fluctuation, respectively. Although the reduction of the turbulence intensity was not so remarkable at $N = 1$, as mentioned earlier, there is a noticeable change in fluctuating pattern. It can be seen in Figure 16(a) that fluctuations with high frequency decrease, and those with low frequency increase in the central region of rotating pipe. In the outer region of the pipe, on the other hand, fluctuations with low frequency decrease, and those with high frequency increase somewhat. The same tendency was seen in the radial velocity fluctuation shown in Figure 13. These facts can be recognized easily in the power spectra shown below. As for the tangential velocity fluctuation shown in Figure 16(b), a distinctive fluctuating pattern appears in the

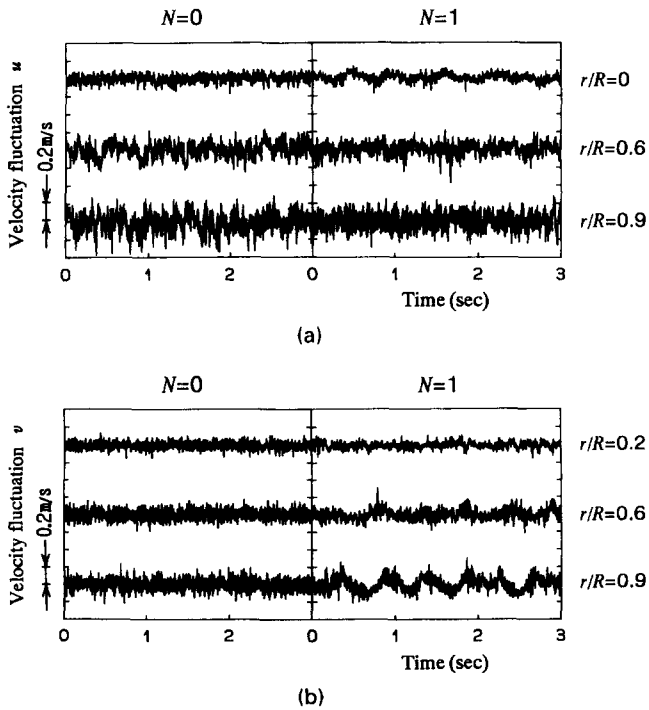

Figure 16 (a) Time records of axial velocity fluctuation (Re= 20000, $z/D = 120$). (b) Time records of tangential velocity fluctuation (Re=20000, $z/D = 120$)

outer region of the pipe. It contains rather periodic large fluctuation with a long cycle. Its cycle is much greater than that of pipe rotation. This fact suggests that the stabilizing effect give rise to a large-scale structure, such as spiral waves that appeared in the laminar region of the rotating pipe (Imao et al. 1992). However, it remains unknown for the present why only the tangential velocity fluctuation shows such periodic large fluctuation in the outer region of the pipe.

Figure 17 shows the power spectra $E_1(k)$, $E_2(k)$, and $E_3(k)$ of the fluctuating velocity component in the axial, tangential, and radial direction, respectively. They are obtained by fast-Fourier transform (FFT). Here the spectra are normalized by $\overline{u^2}$, $\overline{v^2}$, and $\overline{w^2}$, respectively, and k is the wave number in the mean flow direction; i.e.

$$k = \frac{2\pi f}{\sqrt{(U^2 + V^2)}}$$

where f is the frequency. In this study, the analyzed frequency is $f = 0.5 \sim 500$ Hz, and the mean velocity $U_m \sim 0.6$ m/s, so that wavenumbers, for example, at $r/R = 0.9$ and $N = 1$ become $k = 5 \sim 5200$ 1/m. From this figure, it can be seen that in the central region of the rotating pipe the power increases slightly in the range of lower wave number and decreases slightly in the range of middle and higher wave number. In the outer region of the pipe, the power in the range of lower wave number decreases remarkably except for the tangential component. The increase in the power of the tangential component in the range of low wave number corresponds to the periodic fluctuation with low frequency shown in Figure 16(b).

Anwer and so (1989) studied the energy spectrum of the wall shear stress in the flow downstream of the rotating section when the flow with solid-like rotation passes into a stationary pipe. They found that the equilibrium range with a slope of $-5/3$ of the spectrum increased. Because our study is concerned with the fully developed flow in rotating pipe, direct comparison with their data are not be allowed. Nevertheless, when the data are compared for the equilibrium range, the $-5/3$ slope seems to be unaffected in our study, too. On the other hand, the increase or the decrease of the spectrum in the low wave number range is remarkable in our study, which causes the equilibrium range narrower. This difference may arise from the fact that one flow is developed, and the other is damping.

Conclusions

An experimental study was made of the turbulent characteristics of a fully developed flow in an axially rotating pipe. The results are summarized as follows.

(1) Every component of turbulent fluctuations decreases gradually with an increase in rotation rate and the rate of turbulent energy transport in the axial direction is decreased.
(2) Turbulent shear stresses are suppressed more strongly than turbulent kinetic energy, and the momentum transfer by turbulent motion is suppressed in the rotating pipe.
(3) Mixing length is reduced remarkably in the rotating pipe. Its value can be estimated by the use of the coefficient β, which is less than unity, and the Richardson number.
(4) The skewness factor of radial velocity fluctuation approaches 0, and the flatness factor of it increases with an increase in rotation rate due to the stabilizing effect.
(5) In the outer region of the rotating pipe, fluctuations with low frequency decrease except for the tangential component. A rather periodic fluctuation appears with low frequency in the tangential velocity fluctuation.

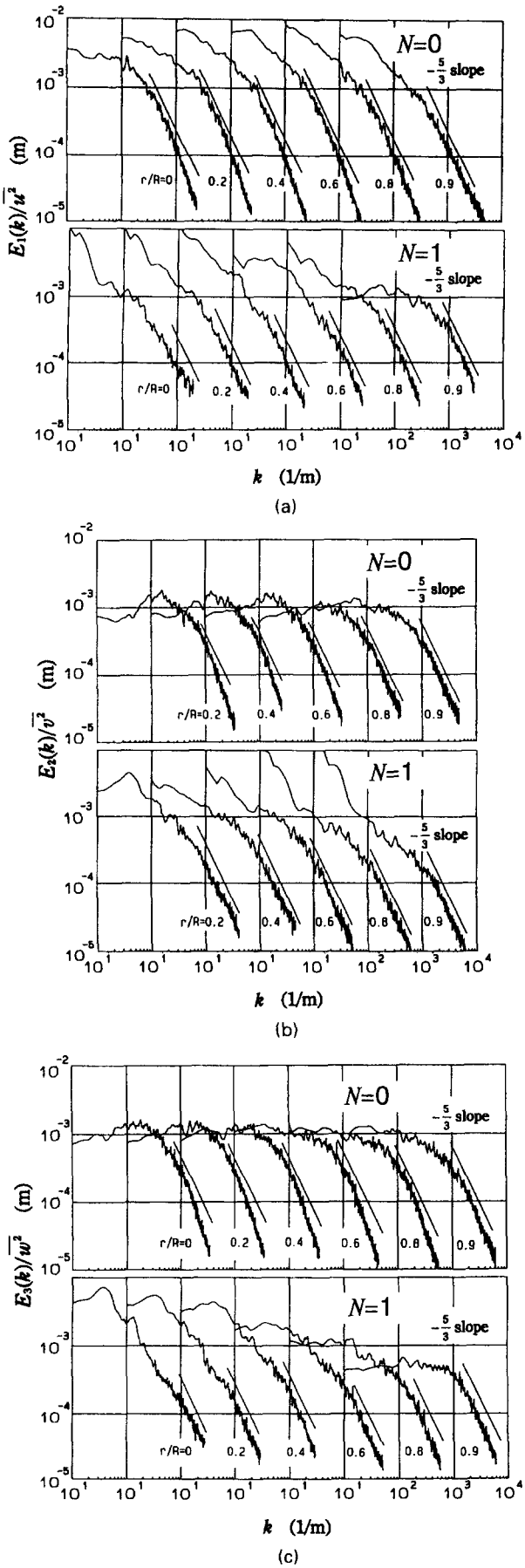

Figure 17 (a) Power spectra of axial velocity fluctuation (Re=20000, $z/D=120$) (uncertainties in $E_1(k)/\overline{u^2}$ and k are ±5%). (b) Power spectra of tangential velocity fluctuation (Re=2000, $z/D=120$) (uncertainties in $E_2(k)/\overline{v^2}$ and k are ±5%). (c) Power spectra of radial velocity fluctuation (Re=20000, $z/D=120$) (uncertainties in $E_3(k)/\overline{w^2}$ and k are ±5%)

Acknowledgment

The authors thank H. Koyama of Tokyo Denki University for the valuable discussion and suggestions.

References

Anwer, M., and So, R. M. C. 1989. Rotation effects on a fully developed turbulent pipe flow. *Exper. Fluids*, **8**, 33–40

Bradshaw, P. 1969. The analogy between streamline curvature and buoyancy in turbulent shear flow. *J. Fluid Mech.*, **36**, 177–191

Hirai, S., Takagi, T. and Matsumoto, M. 1988. Predictions of the laminarization phenomena in an axially rotating pipe flow. *J. Fluids Eng.* **110**, 424–430

Imao, S. 1981. Retransition phenomenon of the flow in an axially rotating pipe (in Japanese). *Bull. Nagoya Inst. Tech.*, **33**, 153–159

Imao, S., Itoh, H., Yamada, Y. and Zhang, Q. 1992. The characteristics of spiral waves in an axially rotating pipe. *Exper. Fluids*, **12**, 277–285

Imao, S., Zhang, Q. and Yamada, Y. 1989. The laminar flow in the developing region of a rotating pipe. *JSME Int. J.* **32**, 317–323

Kikuyama, K., Murakami, M. and Nishibori, K. 1983a. Development of three-dimensional boundary layer in an axially rotating pipe. *J. Fluids Eng.* **105**, 154–160

Kikuyama, K., Murakami, M., Nishibori, K. and Maeda, K. 1983b. Flow in a rotating pipe (A calculation of flow in the saturated region). *Bull. Japan. Soc. Mech. Eng.*, **26**, 506–513

Kitoh, O. 1991. Experimental study of turbulent swirling flow in a straight pipe. *J. Fluid Mech.*, **225**, 445–479

Kline, S. J. and McClintock, F. A. 1953. Describing uncertainties in single-sample experiments. *Mech. Eng.*, **75**, 3–8

Laufer, J. 1954. The structure of turbulence in fully developed pipe flow. *NACA Tech. Rep.* 1174.

Lawn, C. J. 1971. The determination of the rate of dissipation in turbulent pipe flow. *J. Fluid Mech.* **48**, 477–505

Murakami, M. and Kikuyama, K. 1980. Turbulent flow in axially rotating pipes. *J. Fluids Eng.*, **102**, 97–103

Prandtl, L. 1930. Einfluß stabilisierender Kräfte auf die Turbulenz. Vorträge auf dem Gebiete der Aerodynamik und verwandter Gebiete, Springer, Berlin, 1–7

White, A. 1964. Flow of a fluid in an axially rotating pipe. *J. Mech. Eng. Sci.* **6**, 47–52